RSC Advances

ROYAL SOCIETY OF CHEMISTRY

www.rsc.org/advances

Table of Contents

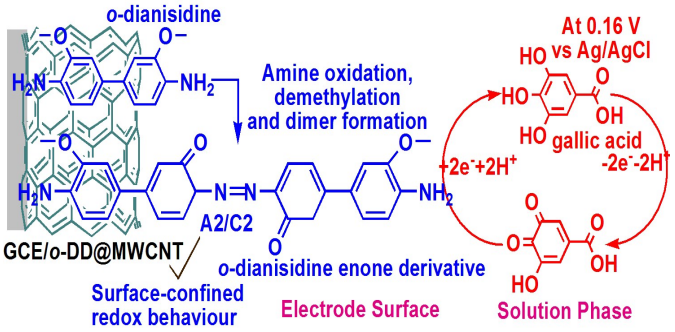

The enone derivative of o-dianisidine dimer stabilized GCE/MWCNT exhibited low potential gallic acid detection at 0.16 V vs Ag/AgCl.

A new electro-generated *o*-dianisidine derivative stabilized MWCNT-modified GCE for low potential gallic acid detection

Sundaram Sornambikai[a], Jagannathan Madhanagopal[a], Mohammed Rafiq Abdul Kadir[a,*], Palanivel Sathishkumar[b], Tony Hadibarata[b] and Abdul Rahim Mohammed Yusoff[b]

[a] *Medical Devices and Technology Group (MEDITEG), Faculty of Biosciences and Medical Engineering, Universiti Teknologi Malaysia (UTM), 81310 Skudai, Johor Bahru, Johor, Malaysia.*

[b]*Centre for Sustainable Environment and Water Security (IPASA), Research Institute for Sustainable Environment, Universiti Teknologi Malaysia, 81310 UTM Skudai, Johor, Malaysia.*

Corresponding author. *E-mail address*: rafiq@biomedical.utm.my; Fax: +6075526222; Tel: +6075535961 (M.R.A. Kadir)

†Electronic Supplementary Information available: Fig. S1. CV responses of GCE/*o*-DD@MWCNT from solution phase prepared hybrid powder and its comparison with the *in-situ* prepared electrode, Fig. S2. Comparison of the GC-MS spectrum of (A) *o*-dianisidine and (B) *o*-DD@MWCNT filtered ethanol extracts, Fig. S3. Effect of the scan rate on the GCE/*o*-DD@MWCNT in the presence of 1 mM GA and Fig. S4. CV response for the effect of the interfering compounds, such as ascorbic acid (AA), uric acid (UA), ellagic acid (EA), dopamine (DA), ferulic acid (FA) and gallic acid (GA) at a concentration of 100 µM, on the GCE/*o*-DD@MWCNT compared to the GCE/*o*-DD@MWCNT blank.

Abstract

The exploration of functional group interactions and electro-generated species stabilization on chemically modified electrodes for efficient electro-analytical application is a continuing research area in electrochemistry. In addition, the electrochemical behaviours of the intermediate species, which are generated from the aromatic organic redox mediator and possess both methoxy and amine functional groups, have been rarely studied for electro-analytical applications. For the first time, we report the stabilization of an electro-generated enone derivative of the *o*-dianisidine (ED*o*-D) dimer formed as one of the intermediate species during *o*-dianisidine immobilization. The electro-generated *o*-dianisidine derivative (*o*-DD)-stabilized multi-walled carbon nanotube (MWCNT)-modified glassy carbon electrode (GCE/*o*-DD@MWCNT) exhibited two highly reproducible and, well-defined surface-confined redox couples in a pH 7 phosphate buffer solution (PBS). FTIR analyses indicated the presence of an amine group linkage and an azo product in the *o*-DD@MWCNT hybrid. UV-Vis and GC-MS analyses confirmed the presence of *o*-dianisidine in its azo dimer form within the MWCNT. In addition, the enone derivative of *o*-dianisidine dimer present on the GCE/*o*-DD@MWCNT successfully sensed gallic acid (GA) at 0.16 V vs Ag/AgCl in pH 7 PBS. Highly selective GA detection was achieved with a sensitivity of 0.4580 $\mu A.\mu M^{-1}$, a detection range of 100-1300 µM and a detection limit of 144 nM using chronoamperometry. GCE/*o*-DD@MWCNT also demonstrated effective GA detection in simulated real grape juice and water samples.

Keywords: carbon nanotube, *o*-dianisidine immobilization, enone derivative, azo dimer, gallic acid.

1. Introduction

Carbon nanotubes (CNTs) and graphite matrices have been explored to immobilize numerous organic redox mediators and stabilize their electro-generated redox products for enhanced electro-analytical applications.[1-8] For example, the redox mediators containing amine,[1,2] methoxy,[3,4] and nitrogen[5,6] functional groups have been immobilized in these nanocarbon matrix-modified glassy carbon electrode (GCE) at a pH of 7. In these chemically modified electrodes, the hydroxyl functional group is generated during continuous potential cycling, and therefore, the intermediate quinone species were stabilized. Similarly, the immobilization of hydroxyl functional group tethered redox mediators is stabilized through an electro-generated quinone within the CNT modified electrodes.[7-9] All of these redox products-stabilized electrodes exhibit highly sensitive, selective, stable and low potential electrochemical sensing for biological analytes.[1-9] However, to the best of our knowledge, the electrochemical immobilization of methoxy tethered aromatic amine based dimer structures and their electro-generated products has not been previously investigated as a mediated sensor system. Therefore, an amine-substituted aromatic benzidine redox mediator (i.e., *o*-dianisidine (3,3'-dimethoxybenzidine)) was studied to develop new electrochemical sensors for sensitive and selective low potential electro-analytical applications.

Since the discovery of *o*-dianisidine, it has been widely used as a substrate for the oxidation of horseradish peroxidase/hydrogen peroxide and aromatic amines as well as dye intermediates and a colourimetric indicator of peroxidase activity.[10-15] Several studies reported that, *o*-dianisidine may produce the following oxidation products during potential cycling: (i) *o*-dianisidine quinonediimine, (ii) amine radical cation containing *o*-dianisidine and (iii) *o*-

dianisidine dimer at a pH ranging from 1 to 11.[10,11,13] In addition, the voltammetry of the electro-oxidized *o*-dianisidine and its redox products is unstable, complicated and non-reproducible at pH>3 due to the formation of multiple intermediate species.[10,11,13] The electro-oxidation of aromatic amine functional groups has resulted in generation of amine radical cations as well as head-to-head amine groups coupling to form dimer monolayers on electrode surfaces.[15,16] Indeed, the dimer monolayers enhanced the stability of the modified electrode system and exhibited excellent electro-analytical application. Studies of the electrochemistry of aromatic methoxy groups indicated that quinone formation occurs via the hydrolysis and demethylation of the methoxy group during potential cycling.[17-20] Therefore, in this study, we aim to understand the behaviour of the electro-oxidized amine and methoxy groups present in *o*-dianisidine within the MWCNT matrix. For this purpose, *o*-dianisidine was immobilized on a multiwalled CNT modified GCE (GCE/MWCNT) via continuous potential cycling at a pH of 7 and further extended to explore its electro-analytical application for the first time. Interestingly, we observed an electro-generated enone form of the *o*-dianisidine dimer rather than the quinone confined to the GCE/MWCNT surface at 0.2 V vs Ag/AgCl. The o-dianisidine derivative stabilized electrode is referred to as GCE/*o*-DD@MWCNT. In addition, physico-chemical and electrochemical characterizations confirmed this unusual mechanism. To extend the modified electrode for electro-analytical applications, gallic acid (GA) was chosen as a model system because GA possesses anti-carcinogenic, anti-mutagenic and antioxidant activities, and therefore, the quantification of GA in the food substances is important for understanding their health benefits.[21,22]

2. Experimental

2.1 Materials and Instrumentation

Pristine-MWCNTs (O.D: <7 nm; I.D: 2-5 nm; length 10-30 μm; >95% purity), *o*-dianisidine and gallic acid anhydrous were purchased from US Research Nanomaterials Inc., Sigma Aldrich (USA) and Merck Schuchardt OHG (Germany), respectively. All of the other chemicals and solvents used in this study were of analytical grade. The atmospheric oxygen containing supporting electrolyte (0.1 M pH 7 PBS) was prepared using double-distilled (DD) water.

Voltammetry was conducted with a VersaSTAT electrochemical workstation, AMETEK (USA). A GCE (0.0707 cm^2 geometric area) and its chemically modified working form as well as a Ag/AgCl reference and graphite rod auxiliary electrodes were used. The following physico-chemical characterizations of *o*-DD@MWCNT were conducted: FTIR/ATR spectroscopy using a Nicolet FTIR spectrophotometer model iD5 (USA), UV-Visible spectroscopy using a Nanocolor®UV/VIS spectrophotometer (USA) and gas chromatography with mass spectrometry (GC-MS) analysis using an Agilent Technologies Gas Chromatograph and Inert Mass Selective Detector 5975 (USA).

2.2 Electrode Preparation

Prior to the experiments, the GCE was mechanically polished as per the BAS polishing kit assay. This step was followed by electrochemical pretreatment using cyclic voltammetry (CV) for n=10, (n = no. of cycles) between -1.0 V and 1.0 V at a potential scan rate (v) of 50 $mV.s^{-1}$ in pH 7 PBS. The MWCNT modified GCE (GCE/MWCNT) was prepared by drop

casting 3 μL of MWCNTs dispersed in ethanol (2 mg.500 μL^{-1}) on the pretreated GCE followed by, air drying for 15 min at room temperature and cycling in the optimal potential window from -0.8 to 0.7 V vs Ag/AgCl for n=20. To prepare the *o*-dianisidine immobilized GCE/MWCNT, the GCE/MWCNT was immersed in 1 mM *o*-dianisidine containing pH 7 PBS for 15 min. The immersed electrode was removed and washed with DD water to remove the MWCNT surface bound *o*-dianisidine and potential cycled in the optimal potential window. For comparison, the bare GCE was immersed in a 1 mM *o*-dianisidine solution, washed and potential cycled (GCE-*o*-dianisidine) in the optimal potential window.

2.3 Samples Preparation for Physico-Chemical Characterization

For FTIR analysis, the *o*-DD@$MWCNT_{powder\ extract}$ hybrid powder was prepared by extracting the electrochemically prepared GCE/*o*-DD@MWCNT in 5 mL of ethanol followed by removing the ethanol under vacuum prior to analysis. The preparation of the electrode was repeated 20 times in the optimal potential window to obtain a considerable amount of hybrid powder for FTIR/ATR analysis. For the UV-Vis and GC-MS analyses, the GCE-*o*-dianisidine and GCE/*o*-DD@MWCNT was individually ultrasonicated in 3 mL of 50% ethanol. Then, the extracts were filtered using a 0.45 μm syringe filter in 5 mL disposable syringes.

2.4 Real Sample Preparation

For the real sample analysis, the red grape juice (#1) purchased from the nearby local market and tap water (#2) from the biomaterials degradation laboratory, UTM, Johor was utilized. 2 g of red grapes were weighed and homogenized with 10 mL of pH 7 PBS using a mortar and pestle. First, this solution was filtered and suitably diluted with pH 7 PBS (dilution

factor = 3). For the tap water sample, the water was filtered and diluted with pH 7 PBS at a dilution factor of 3. For the real sample analysis, 10 mL of the prepared real sample solutions were taken, and different concentrations of GA were added from the prepared 1 mM GA containing real sample stock solutions using a standard addition approach. GA quantification of real samples in the absence and presence of known concentrations of added GA was carried out using chronoamperometry.

3. Results and Discussion

3.1. Electrochemical Behaviour of o-Dianisidine Immobilized GCE/MWCNT

To examine the electrochemical behaviour of *o*-dianisidine immobilized GCE/MWCNT, the modified electrode was subjected to potential cycling in different potential windows in pH 7 PBS (data not shown). Interestingly, the modified electrode exhibited two well-defined redox behaviours for the potential window ranging from -0.8 to 0.7 V vs Ag/AgCl, as shown in Fig. 1A. This potential window was determined to be optimum for further studies. In the optimal potential window, in the first cycle of CV, the modified electrode exhibited an irreversible oxidation peak (A′ (0.34 V) vs Ag/AgCl) during the positive potential sweep with two reduction peaks (C2 (0.29 V) and C1 (-0.36 V)) during the negative potential sweep. In the 2^{nd} cycle, a new anodic peak at -0.36 V (A1) appeared with an increasing peak current, which saturated after the 10^{th} cycle. In addition, saturation in the peak currents corresponding to the reduction (C1) peak and irreversible oxidation (A′) peak that gradually disappeared to form A2 was simultaneously observed. With a further increase in potential cycles to n=20, both the (A1/C1) and (A2/C2) redox couples exhibited a potential shift in the negative direction. The A1/C1 (-0.37 V/-0.39 V) and A2/C2 (0.207 V/0.179 V) redox couples for the last 10 cycles, which exhibit saturation in

the peak currents, are shown in Fig. 1B. The relative standard deviation (RSD: %) for the last 10 CV cycles was 3.6%, which indicates a stable redox mediated system and stable adsorbed *o*-dianisidine species on the electrode surface. Therefore, *o*-dianisidine may act as a redox mediator that results in well-defined surface-confined redox couples on the GCE/MWCNT, and this modified electrode is referred to as GCE/*o*-DD@MWCNT. The calculated peak-to-peak separation ($\Delta E_p = E_{pa}$-E_{pc}, pa and pc corresponding to the anodic and cathodic peak currents) and apparent standard electrode potential ($E^{o\prime} = (E_{pa}+E_{pc})/2$) values were 0.02±0.002 V and 0.38±0.002 V for A1 and C1 respectively and 0.028±0.001 V and 0.193±0.01 V for A2 and C2, respectively at 50 $mV.s^{-1}$. The number of electrons (n) for the redox behaviour of *o*-dianisidine immobilized MWCNT-modified electrode is 2. The low ΔE_p suggested the fast electron transfer involved in this electrode system. The calculated E_{pa}-$E_{pa/2}$ values were 0.149±0.0002 V and 0.120±0.0002 V and the calculated anodic to cathodic peak current ratios (i_{pa}/i_{pc}) were 0.67 and 1.17 for A1/C1 and A2/C2, respectively at 50 $mV.s^{-1}$.

To examine the stability and reproducibility of the *in-situ* prepared GCE/*o*-DD@MWCNT, ten individual CV experiments were carried out under optimal conditions. This system also exhibited nearly consistent A1 and A2 peak currents, as shown in the inset of Fig. 1B. The calculated RSD % values for all ten experiments were in the range of 3.5 to 4.0 %. These observations indicated that the voltammetric behaviour of the *o*-dianisidine immobilized electrode is highly stable and reproducible, which is in contrast to unstable and non-reproducible voltammetry of *o*-dianisidine on modified electrodes that has been previously reported.[10,13] Similarly, the stable and reproducible redox behaviours were observed only in the presence of the MWCNT matrix and not on the bare GCE modified with *o*-dianisidine. The bare GCE-

immobilized with *o*-dianisidine under the same experimental conditions (GCE-*o*-dianisidine) for n=20, exhibited only feeble electrochemical behaviour for *o*-dianisidine, as shown in Fig. 1C. This observation indicated the significance of the MWCNT matrix that was utilized for *o*-dianisidine immobilization on the GCE in this study. In addition, to determine the location of *o*-dianisidine in the MWCNT matrix, the *o*-DD@MWCNT$_{solnphase}$ hybrid powder was prepared by initially making an ethanol suspension with 2 mg of both MWCNT and *o*-dianisidine followed by ultrasonication for 30 min at room temperature. The solution phase prepared hybrid powder was obtained after washing the suspension to remove the loosely adsorbed *o*-dianisidine (i.e., washing were continued until a negative signal was observed for *o*-dianisidine using UV-Vis spectroscopy) and dried under vacuum overnight.[7] This solution phase prepared hybrid powder was drop casted on GCE and dried for 15 min. Then, the electrochemical behaviour of GCE/*o*-DD@MWCNT$_{solnphase}$ was examined by continuous potential cycling in the optimal potential window. The GCE/*o*-DD@MWCNT$_{solnphase}$ exhibited qualitatively similar redox patterns as the *in-situ* prepared electrode with a RSD of 4.8%, as shown in Fig. S1†. This qualitative similarity suggested the existence of fractions of electroactive *o*-dianisidine derivative species within the MWCNT matrix.[7]

3.2. Possible Mechanism for o-DD Stabilization

To identify the nature of the electro-oxidized intermediate products that are responsible for the immobilization of *o*-dianisidine in this study, the *o*-dianisidine immobilized GCE/MWCNT was examined in three different potential windows in pH 7 PBS, as shown in Fig. 1D. If the anodic oxidation of *o*-dianisidine is responsible for the formation of the redox couples, no redox behaviour is expected to be observed during potential cycling below +0.2 V. In

agreement with this hypothesis, no redox behaviour was observed based on CV between -0.5 V and +0.1 V (Fig. 1D (a)). However, when the potential window was extended to +0.3 V, the oxidation peak appeared at +0.22 V, which produced a feeble redox couple at -0.36 V (A1/C1) and a strong redox couple at ~0.2 V (A2/C2), as shown in (Fig. 1D (b)). This observation suggested that the electro-oxidation of the amine functional group present in *o*-dianisidine produced an amine radical cation[1,16] and conjugated electron donation of the methoxy group to the *o*-dianisidine may have resulted in the formation of the A1/C1 redox couple. If the quinone product was formed on the electrode at a negative potential during continuous cycling, a well-defined redox couple responsible for quinone would be observed at -0.2 V due to the OH generation and immobilization within the electrode surface.[1-8] In addition, quinone formation from the electrochemical conversion of a methoxy group to a hydroxyl group occurs via a ketone group at acidic and alkaline pH.[3,4] This type of conversion occurred only in the presence of a hydroxyl group located in the carbon ring of the parent compound in the *ortho* position of the methoxy group.[3,4]

To determine the possibility for direct conversion of the methoxy group present in *o*-dianisidine to a hydroxyl group in the absence of any hydroxyl functional groups in the chemical structure of the parent *o*-dianisidine, CV was carried out between -0.1 V and 0.7 V. At this stage, no reversible peaks were expected for the direct demethylation to the hydroxyl functional group. Interestingly, the appearance of anodic oxidation peak at +0.22 V gradually decreased and a strong redox couple (A2/C2) was observed at 0.2 V, which ruled out the possibility of direct demethylation to the hydroxyl group (Fig. 1D (c)). Therefore, the observed redox behaviours may be due to amine group oxidation, and the possibility of OH formation and its further

conversion to quinone was ruled out. In addition, the A2/C2 peak did not continue to increase with increasing potential cycles in the optimal potential window, as observed for aniline.[1] Therefore, no polymerization occurred, and therefore, the oxidized amine radical cation may be involved in electron delocalization and further hydrolysis and demethylation to form the ketone functional group at the *ortho* position in *o*-dianisidine. With this background, the two redox behaviours of GCE/*o*-DD@MWCNT may be assigned as (i) an A1/C1 redox couple, where the demethylation and electron delocalization of the amine radical cation with the methoxy group occurred, and (ii) an A2/C2 redox couple, where the formation of the enone derivatized *o*-dianisidine dimer and its reversible electron transfer with a hydroxyl tethered at one end of the dimer is expected. In addition, physico-chemical characterizations were conducted using FTIR, UV-Vis and GC-MS spectroscopy to confirm the proposed redox products.

3.3. Physico-chemical Characterization

The possible functional group interactions involved between *o*-dianisidine and MWCNTs were investigated by subjecting the *o*-DD@MWCNT$_{\text{powder extract}}$ hybrid powder (a), *o*-dianisidine (b) and MWCNTs (c) to FTIR analysis (ATR Mode) in the range of 600 to 4000 nm. The *o*-DD@MWCNT$_{\text{extract}}$ hybrid powder exhibited a combination of *o*-dianisidine and MWCNT FTIR patterns, as shown in Figs. 2A and B. The stretching vibrations were observed at 1238 and 1282 (C—N), 1700 and 1730 (C=O), 1760 (C=N), 1530, 1630 and 1650 cm^{-1} (N—H) for the aromatic amine group of *o*-dainisidine.[23] The azo —N=N— and aromatic O—H stretching vibrations were observed at 1585, and 3600 cm^{-1}, respectively.[23] A band at ~2000 cm^{-1} that corresponds to the aromatic combination peak was also observed for both the MWCNTs and the hybrid (Fig. 2A). These observations are consistent with the interactions between *o*-dianisidine and the MWCNT

matrix as an azo dimer and its enone form with the hydroxyl functional group involved. To confirm the presence of the azo dimer form of *o*-dianisidine in the hybrid, the UV-Vis spectrum of *o*-DD@MWCNT and native *o*-dianisidine filtered extracts were analysed in the 200-700 nm range. The comparison spectrum exhibited two prominent wavelength peaks at 282 and 301 nm (inset in Fig. 2C), which are characteristics of the *o*-dianisidine oxidation spectra.[24] The oxidation product of *o*-dianisidine was also identified based on a strong colour change from white to reddish yellow due to the azo functional group (inset photograph in Fig. 2C).[25] However, bare *o*-dianisidine did not produce a colour change. This observation indicated the enhanced oxidation and dimer formation of *o*-dianisidine in the presence of the MWCNT matrix. In addition, the azo form of the dimer peak was also observed at 422 nm, as shown in Fig. 2C, which is in agreement with the literature result.[25]

To further validate the presence of the dimer and identify the oxidation products produced during the *o*-DD@MWCNT hybrid formation, GC-MS analysis was carried out for the filtered ethanol extract of the hybrid material in the following sequence: (i) The detector was injected with helium gas at a flow rate of 1.1 $ml.min^{-1}$, and the injection temperature was maintained at 300 °C; (ii) The oven was maintained at 100 °C for 2 min, and then, the temperature was increased to 250 °C at a heating rate of 10 °C min^{-1}; and (iii) Finally, the temperature was increased up to 280 °C at a heating rate of 30 °C min^{-1}. For comparison, the mass spectrum of the bare *o*-dianisidine oxidation products is shown in Fig. S2A†. The filtered *o*-dianisidine extract exhibited a characteristic mass spectrum with an m/z value of 244.1 at a retention time (R_T) of 12.534 s. However, the mass spectrum of the filtered hybrid extract exhibited a prominent peak at R_T = 12.723 s with a m/z = 229, as shown in Fig. S2B†. This mass

value may correspond to the hydroxyl functional group attached to *o*-dianisidine, which is formed from hydrolysis and demethylation. An additional mass peak at R_T = 13.336 s with m/z = 458.9 (M-1) was observed for the hybrid, as shown in Fig. 2D. The enone derivative of *o*-dianisidine (ED*o*-D) may be responsible for the appearance of this peak. The other oxidation peaks observed in the GC-MS spectrum may be due to the electro-inactive products in the hybrid system.

Based on the FTIR, UV-Vis and GC-MS results along with the electrochemical behaviour of *o*-DD@MWCNT, a possible mechanism for the stabilization of *o*-DD in the MWCNT modified electrode has been proposed. The proposed electrochemical oxidation and reduction mechanism (Scheme 1) involves the generation of an irreversibly oxidized amine radical cation (A′) during the positive potential sweep.[15] Then, the delocalization of the radical cation followed by oxidative demethylation leads to the conversion of the methoxy group to a keto group in the *ortho*- position on one end of *o*-dianisidine.[18,26] Next, electron hopping may occur, and the keto group could convert the hydroxyl group to more amine radical cations during continuous potential cycling. This step may be followed by amine group head-to-head coupling, which resulted in a NH—NH and —N=N— linked dimer and its enone form, respectively. The formation of this enone derivatized *o*-dianisidine dimer during electrochemical cycling is unique to this study. The possible electron transfer mechanism of the *o*-DD stabilized electrode was studied further.

3.4. Electrochemical Characterization of GCE/o-DD@MWCNT

The possible electron transfer mechanism involved in the modified system was analysed based on the effect of the scan rate (*v*) on the GCE/*o*-DD@MWCNT, and the results are shown

in Fig. 3A. The scan rates were varied from 5-500 $mV.s^{-1}$ in pH 7 PBS, and a linear increase in the i_{pa} as v increased (Fig. 3A) and symmetric behaviour of the redox peaks were observed. The $\partial \log i_{pa}/\partial \log v$ values for the A1 and A2 peaks were 0.9±0.05 and 0.87±0.06, respectively, as shown in Fig. 3A (inset). These values are closer to the adsorption controlled electron transfer mechanisms and therefore, an adsorption mechanism was observed in the modified system. To understand the nature of the proton-electron transfer for GCE/*o*-DD@MWCNT, the electrode was subjected to potential cycling for n=1 with pH values ranging from 2 to10. The pH values were varied by adding drops of 1 M NaOH and 1 M HCl. As shown in Fig. 3B, the redox peak potentials were shifted in a negative direction as the solution pH increased. Two stable and prominent A1/C1 and A2/C2 redox couples with high peak currents were observed at a pH of 7. However, the typically employed acidic pH resulted in a feeble redox couple (A1/C1) in the negative potential. As shown in Fig. 3B (inset), the calibration plot between the peak potential and solution pH resulted in $\partial E_{pa}/\partial pH$ values of 69 (A1/C1) and 64 $mV.pH^{-1}$ (A2/C2), which revealed the non-Nernstian and Nernstian electron transfer behaviours, respectively. Finally, the detection of 1 mM GA by the GCE/*o*-DD@MWCNT electrode was investigated in pH 7 PBS to evaluate its potential for use as an electrochemical sensor.

3.5. Gallic Acid Detection

Earlier studies on the electrochemical detection of GA either utilized enzymes, linkers with time consuming electrode preparation procedures or higher oxidation potentials.[21,27-33] Therefore, a simple, enzyme-less and linker-less chemically modified electrode is necessary for the detection of GA at low potentials. Herein, a low potential, highly selective, sensitive and nanomolar GA detection has been demonstrated on a novel *o*-dianisidine derivative stabilized

MWCNT modified GCE at neutral pH. The comparative CV responses of 1 mM GA on the (a) GCE, (b) GCE-*o*-dianisidine, (c) GCE/MWCNT and (e) GCE/*o*-DD@MWCNT modified electrodes, are shown in Fig. 4A. Curve d in Fig. 4A is the CV response of GCE/*o*-DD@MWCNT in blank PH 7 PBS in the absence of GA. The unmodified electrodes did not exhibit a significant GA detection peak. However, GCE/MWCNT (curve c) exhibited a 20 μA oxidation peak current at 0.15 V, and GCE/*o*-DD@MWCNT yielded a 44 μA peak current signal at 0.16 V vs Ag/AgCl at the A2/C2 redox couple potential (curve e). The scan rates varied from 5-500 $mV.s^{-1}$ in pH 7 PBS, for the GCE/*o*-DD@MWCNT electrode in the presence of 1 mM GA, and this electrode exhibited a linear increase in i_{pa} as v increased (Fig. S3†) at 0.16 V vs Ag/AgCl. The $\partial i_{pa}/\partial v$ value for the A2 peak was 0.59±0.01, as shown in Fig. S3 (inset). This value indicated the diffusion controlled electron transfer mechanisms between the modified system and gallic acid.

In addition, the effect of [GA] on the CV of the GCE/*o*-DD@MWCNT electrode (Fig. 4B) resulted in two linear ranges (i.e., 0 μM -500 μM and 600 μM -1 mM) for GA (R^2=0.968) with a calculated detection limit (LOD) of 586 nM. The GCE/*o*-DD@MWCNT electrode resulted in a highly selective GA detection response without any interference from ascorbic acid, dopamine, ferulic acid, ellagic acid and uric acid at 0.16 V. The effect of interferences was confirmed using CV at a 100 μM concentration of each of the interfering compounds, and the results are shown in Figs. 5A-F. The CV response of GCE/*o*-DD@MWCNT in the presence of these analytes each at a concentration of 100 μM compared to the modified electrode in the absence of analytes is shown in Fig. S4. The *o*-dianisidine derivative stabilized MWCNT-

modified electrode proposed in this work was highly selective for GA detection at 0.16 V vs Ag/AgCl.

In addition, the typical chronoamperometry responses in the absence and presence of GA using the standard addition methodology with the GCE/*o*-DD@MWCNT electrode at an applied potential of 0.16 V vs Ag/AgCl for duration of 100 s are shown in Fig. 6A. A substantial increase in the peak currents was observed with the standard addition of 100 μM GA until 1.3 mM in the pH 7 PBS. The calibration plot for the peak current value taken at the 100th second as a function of the GA concentration yielded a sensitivity value of 0.458 μA.μM^{-1} with a linear detection range of 100 to1300 μM, and the calculated detection limit obtained for the lowest concentration was 144 nM. This GA detection potential and limit of detection (LOD), which are compared to previous results,[21,27-34] in Table 1, are the advantages of this linker-less, enzyme-less, simple and highly selective new electrochemical sensor at neutral pH.

To investigate its practical application, the new GCE/*o*-DD@MWCNT electrode was employed for GA detection in simulated real grape juice and water samples using chronoamperometry. In addition to the health benefits of GA, a large quantities of GA released to the environment from food and, pharmaceutical industries as well as distilleries may produce harmful oxidized products that can contribute to acid rain.[35] Therefore, its detection in the environment is crucial. Herein, the competence of the modified electrode to detect GA in the real samples was tested, and the results are shown in Fig. 6B. Two real samples, (i.e., grape juice (#1) and water (#2)) were examined in this study, and the results are summarized in the Table 2. The modified electrode exhibited appreciable apparent recovery values in the range of 99 to 100 % for three different GA added concentrations (100-300 μM) using chronoamperometry at 0.16 V.

The stability and reproducibility of the GCE/*o*-DD@MWCNT electrode to detect GA in real samples are shown in Figs. 6C and 6D. The proposed electrode was highly stable and reproducible for sensing GA in the real samples for three consecutive additions of 100, 200 and 300 μM GA. The kinetics and mechanistic studies of the GCE/*o*-DD@MWCNT stabilization and its GA sensing are under way.

4. Conclusions

This study is unique in the following aspects: (i) a new method was developed to trap enone derivative dimeric functional group intermediates which is a new electrochemistry concept; (ii) an atypical enone derivative of the *o*-dianisidine dimer redox product was generated electrochemically on a MWCNT-modified GCE, and two well-defined surface-confined redox behaviours were identified; (iii) the electro-oxidized amine radical cation and methoxy functional groups generated a hydroxyl group via delocalization and demethylation that may be involved in the immobilization of *o*-dianisidine as a redox mediated electrode system; (iv) interpretation of the voltammetric behaviour of *o*-dianisidine at neutral pH was achieved; (v) low potential, highly selective, sensitive and nanomolar detection of gallic acid at neutral pH was demonstrated and extended to real samples; and (vi) a new approach for the use of methoxy aniline based organic compounds for the development of efficient sensors.

Acknowledgements

S.S. and P.S. wish to thank UTM, for providing post-doctoral research fellowships. M.R.A.K acknowledges the FRGS grant (R.J130000/7845/4F581). S.S gratefully acknowledges the valuable suggestions given by Prof. Annamalai Senthil Kumar, Vellore Institute of Technology,

India and Dr. Baskar Selvaraj and Mr. Senthil Kumaran, National Tsing-Hua University, Taiwan.

Notes and References

1 N. Vishnu, A.S. Kumar, K.C. Pillai, *Analyst*, 2013, **138**, 6296-6300.

2 N. Chauhan, J. Narang, C.S. Pundir, *Analyst*, 2011, **136**, 1938-1945.

3 B. Grundig, G. Wittstock, U. Rudel, B. Strhlitz, *J. Electroanal. Chem*., 1995, **395**, 143-157.

4 H.R. Zare, M. Tashkili, H. Khoshro, D. Nematollahi, A. Benvidi, *Anal. Methods*, 2014, **6**, 5999-6008.

5 X.Mao, Y. Wu, L. Xu, X. Cao, X. Cui, L. Zhu, *Analyst,* 2010, **136**, 293-298.

6 P. Gayathri, A.S. Kumar, *Langmuir*, 2014, **30**, 10513-10521.

7 S. Sornambikai, A.S. Kumar, J. Madhanagopal, M.R.A. Kadir, *Anal. Methods*, 2014, **6** 8894-8900.

8 A.S. Kumar, S. Sornambikai, S. Venkatesan, J.-L. Chang, J.-M. Zen, *J. Electrochem. Soc*., 2012, **159**, G137-G145.

9 P. Gopal, T.M. Reddy, C. Nagaraju, G. Narasimha, *RSC Adv.*, 2014, **4**, 57591–57599.

10 J. Jasnowska, M. Ligaj, B. Stupnicka, M. Filipiak, *Bioelectrochemistry*, 2004, **64**, 85-90.

11 P.D. Josephy, T. Elling, R.P.Mason, *J. Biol. Chem*, 1982, **257**, 3669-3675.

12 T.M. Lizier, M.V.B. Zanoni, *Molecules*, 2012, **17**, 7961-7979.

13 Z. Shen, V.D. Parker, A.E. Aust, *Anal. Chem*., 1995, **67**, 307-311.

14 M.C. Icardo, J.V.G. Mateo, J. M. Calatayud, *Analyst*, 2001, **126**, 2087-2092.

15 A. Claiborne, I. Fridovich, *Biochemistry*, 1979, **18**, 2324-2330.

16 S. Baskar, C.-W. Liao, J.-L. Chang, J.-M. Zen, *Electrochim. Acta,* 2013, **88**, 1-5.

17 A. Mardegan, V. Pifferi, E. Pontoglio, L. Falciola, P. Scopece, L.M. Moretto, *Electrochem. Commun*., 2014, **48**, 13-16.

18 M.J. Sims, Q. Li, R.T. Kachoosangi, G.G. Wildgoose, R.G. Compton, *Electrochim. Acta,* 2009, **54**, 5030-5034.

19 Y. Yardim, Z. Senturk, *Talanta*, 2013, **112**, 11-19.

20 E.P. Randviir, J.P. Metters, J. Stainton and C.E. Banks, *Analyst*, 2013, **138**, 2970-2981.

21 J.H. Luo, B.L. Li, N.B. Li, H.Q. Luo, *Sens. Actuat. B. Chem*., 2013, **186**, 84-89.

22 K.E. Yaknovleva, S.A. Kurzeev, E.V. Stepanova, T.V. Federova, B.A. Kuznetsov, O.V. Koroleva, *Appl. Biochem. Microbiol.*, 2007, **43**, 661-668.

23 J. Coates, in *Interpretation of Infrared spectra, A Practical Approach*, Encyclopedia of Analytical Chemistry, ed. R.A. Meyers, John Wiley & Sons Ltd, Chichester, 2000, pp. 10815-10837.

24 N.A. Bagirova, T.N. Shekhovtsova, R.B. van Huystee, *Talanta*, 2001, **55**, 1151-1164.

25 S.B. Maddinedi, B.K. Mandal, *Austin J Anal. Pharm. Chem.*, 2014, **1**, 1-4.

26 R.S. Kim, W. Park, H. Hong, T.D. Chung, S. Kim, *Electrochem. Commun*., 2014, **41,** 39-43.

27 S.M. Ghoreishi, M. Behpour, M. Khayatkashani, M.H. Motaghedifard, *Anal. Methods,* 2011, **3,** 636-645.

28 O. Makhotkina, P.A. Kilmartin, *Anal. Chim. Acta*, 2010, **668**, 155-165.

29 N.S. Sangeetha, S.S. Narayanan, *Anal. Chim. Acta*, 2014, **828**, 34-45.

30 L.P. Souza, F. Calegari, A.J.G. Zarbin, L.H.M. Junior, M.F. Bergamini, *J. Agric. Food. Chem*. 2011, **59**, 7620–7625.

31 R. A.-Hamid, E.F. Newair, *J. Electroanal. Chem*., 2013, **704**, 32-37.

32 V. Carralero Sanz, M. Luz Mena, A. Gonzalez-Cortes, P. Yanez-Sedeno, J.M. Pingarron, *Anal. Chim. Acta*, 2005, **528**, 1–8.

33 C. Lanzellotto, G. Favero, M.L. Antonelli, C. Tortolini, S. Cannistraro, E. Coppari, F. Mazzei, *Biosens.Bioelectron.*, 2014, **55**, 430-437.

34 J. Tashkhourian, S.F. Nami-Ana, *Mater. Sci. Engg. C*, 2015, Accepted manuscript, doi: 10.1016/j.msec.2015.03.017.

35 R. Melo, J.P. Leal, E. Takács, L. Wojnárovits, *J. Hazard. Mater.* 2009, **175**, 1185-1192.

Figure Captions

Figure 1. (A) Twenty continuous CV responses of GCE/MWCNT in blank pH 7 PBS after immersion in 1 mM *o*-dianisidine/PBS. (B) Ten continuous CV responses of the *in-situ* prepared GCE/MWCNT electrode modified with *o*-dianisidine, and the number of repetitions as a function of the A1 and A2 peak currents is shown in the inset. (C) Twenty continuous CV responses of GCE-*o*-dianisidine. (D) CV responses for n=10 with the GCE/MWCNT electrode modified with *o*-dianisidine in three different potential windows. All scans at υ=50 mV.s^{-1}.

Figure 2. (A and B) FTIR patterns of (a) MWCNT, (b) *o*-dianisidine and (c) *o*-DD@MWCNT$_{\text{powder extract}}$ hybrid powder. (C) UV-Vis spectrum of *o*-dianisidine and *o*-DD@MWCNT filtered ethanol extracts. The insets in figure C are; a photograph of the *o*-dianisidine (white) and *o*-DD@MWCNT (reddish yellow) filtered ethanol extracts obtained from the respective electrodes, and the UV-Vis spectrum is enlarged for clarity. (D) GC-MS spectrum of the *o*-DD@MWCNT filtered ethanol extract.

Figure 3. (A) Effect of v and (B) pH on the GCE/*o*-DD@MWCNT electrode. The inset plots contain (i) the calibration plot between log i_{pa} of the A1 and A2 peaks as a function of v (Fig. 3A) and (ii) the calibration plot between E_{pa} of the A1 and A2 peaks as a function of pH (Fig. 3B). [*o*-dianisidine] = 1 mM.

Figure 4. (A) CV response of the GCE/*o*-DD@MWCNT electrode in the absence (d) and presence (e) of [GA] = 1 mM in pH 7 PBS compared to the unmodified electrodes (a-c). (B) Effect of [GA] on GCE/*o*-DD@MWCNT at v=10 mV.s^{-1}.

Figure 5. Individual CV responses for the effect of interfering compounds (100 μM concentration) including (A) gallic acid (GA), (B) ferulic acid (FA), (C) uric acid (UA), (D) dopamine (DA), (E) ellagic acid (EA) and (F) ascorbic acid (AA), on the GCE/*o*-DD@MWCNT electrode compared to the GCE/*o*-DD@MWCNT electrode without analytes. All scans at υ = 10 $mV.s^{-1}$ and n=1. *The scale is enlarged to focus on the oxidation potentials of the analytes*.

Figure 6. (A) Chronoamperometry response for the GCE/*o*-DD@MWCNT electrode in the absence and presence of [GA] = 0 μM-1.3 mM (varying with 100 μM addition), and the inset shows the corresponding calibration plot. (B) Chronoamperometry response of GCE/*o*-DD@MWCNT in the absence and presence of GA in the grape juice and water samples, [GA]=100 μM-300 μM. (B) Triplet chronoamperometry response of GCE/*o*-DD@MWCNT in the water sample using the standard addition approach for GA detection, [GA]=100 μM-300 μM. and (C) Triplet chronoamperometry response of GCE/*o*-DD@MWCNT in the grape juice sample using standard addition approach for GA detection, [GA]=100 μM-300 μM. The chronoamperometry parameters are as follows: potential = 0.16 V, time period = 100 s and points per second = 0.5.

Figure 1

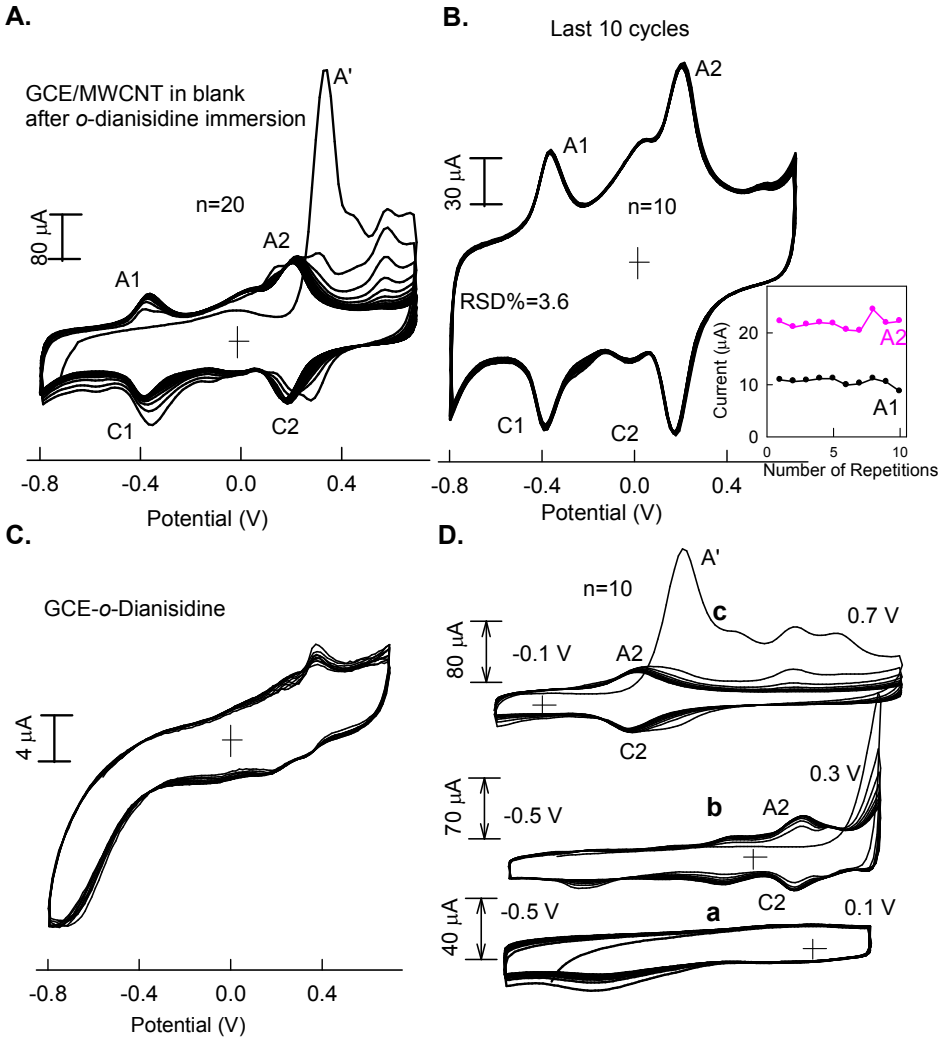

Figure 2

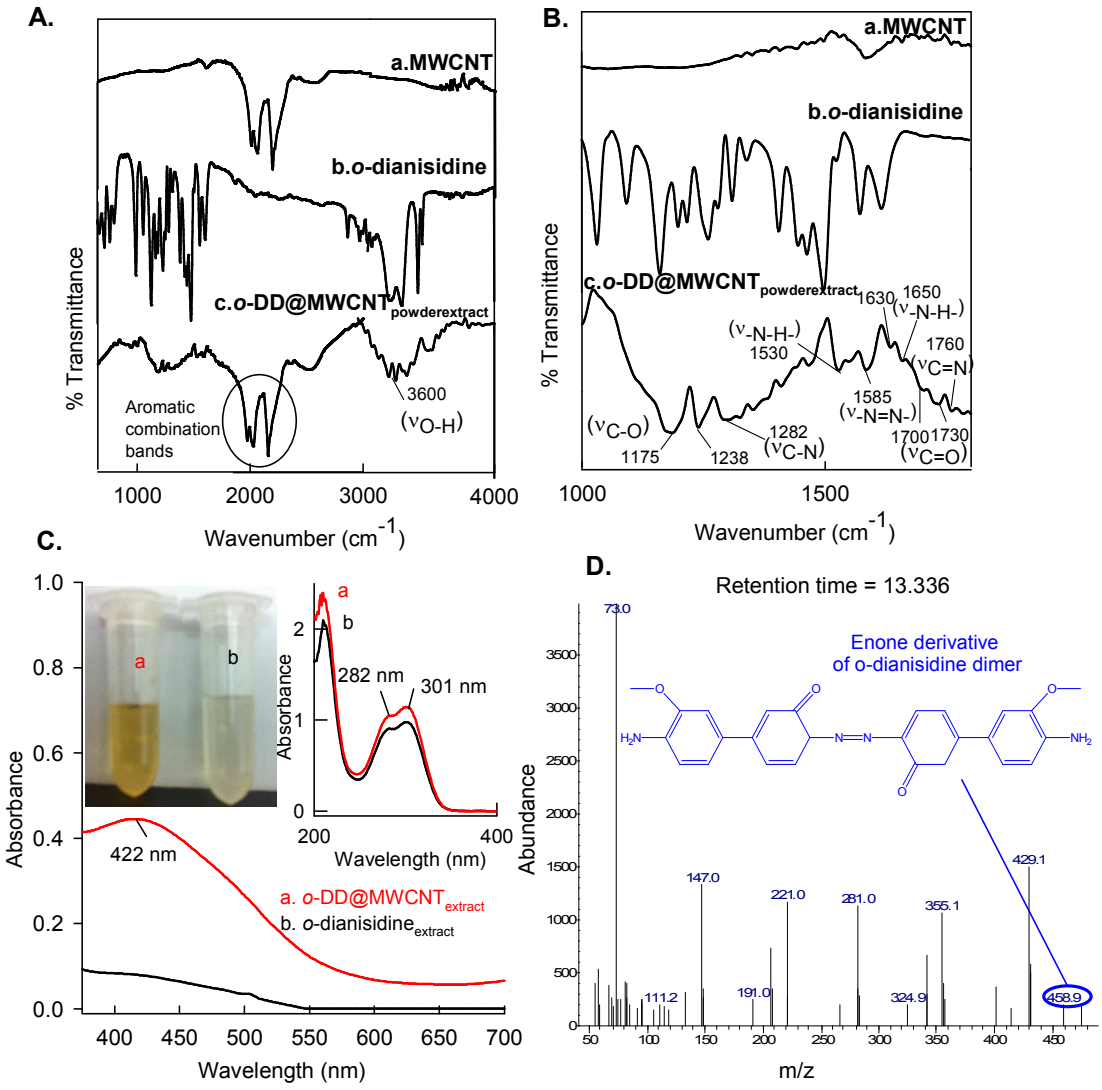

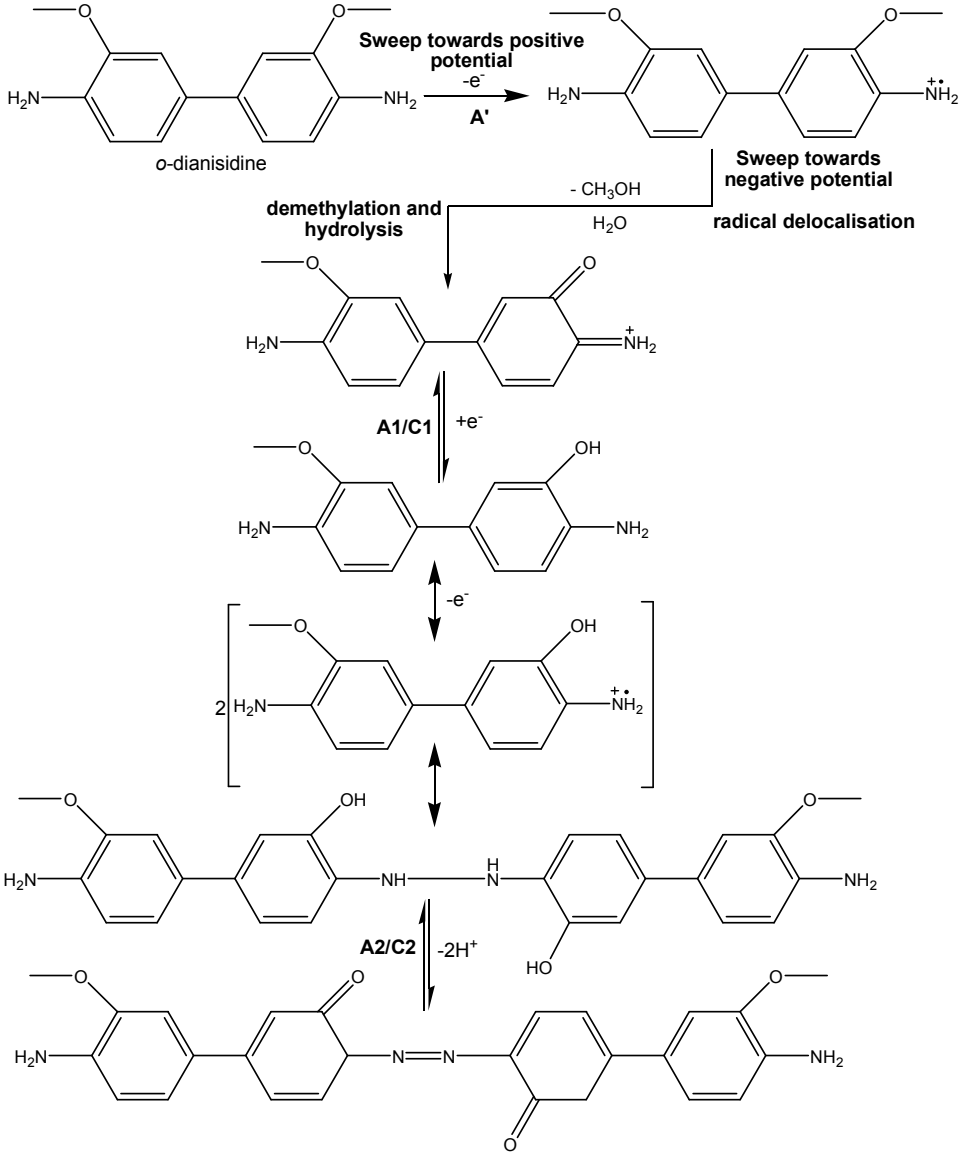

Scheme 1. Schematic representation for the formation of possible electro-generated *o*-dianisidine derivatives (*o*-DD) on GCE/MWCNT during *o*-dianisidine immobilization through continuous potential cycling in pH 7 PBS.

Figure 3

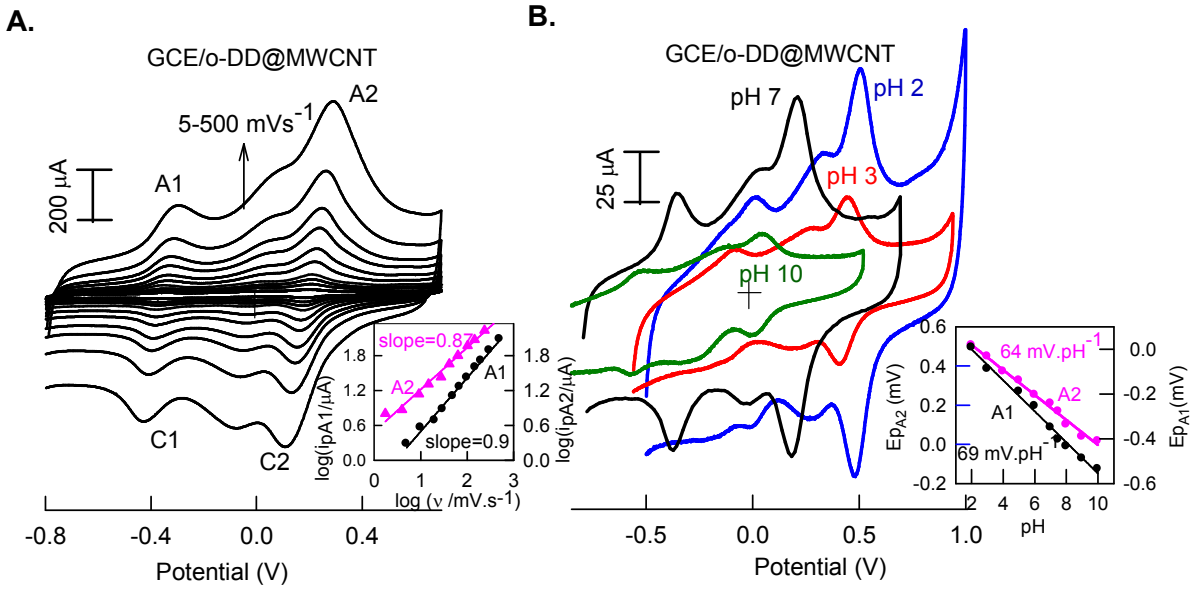

Figure 4

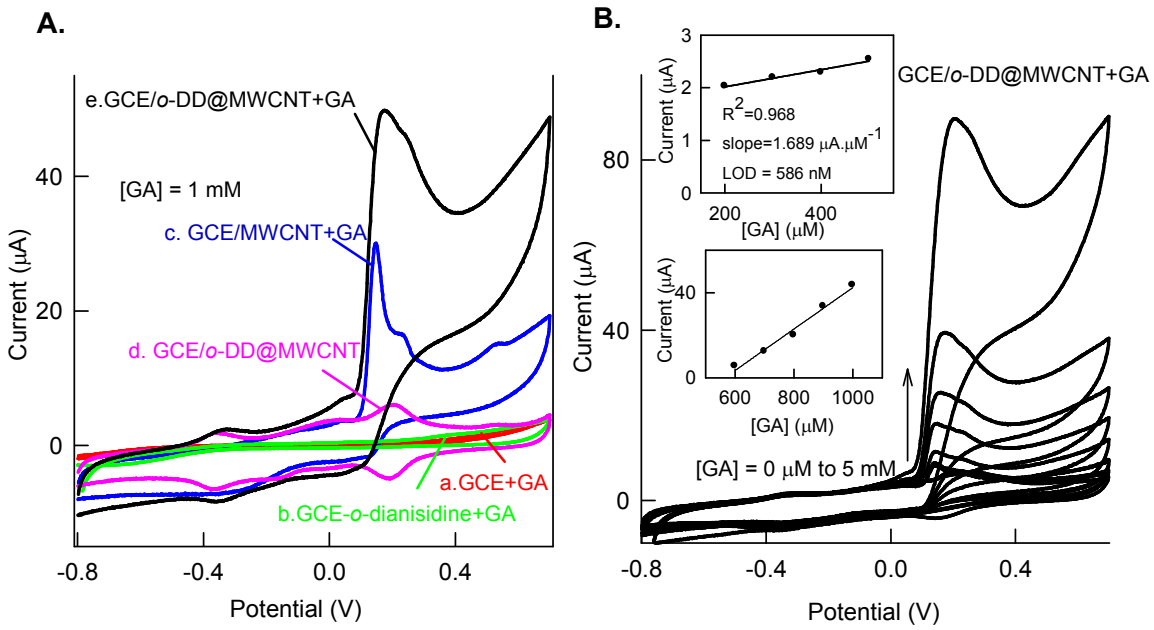

Figure 5

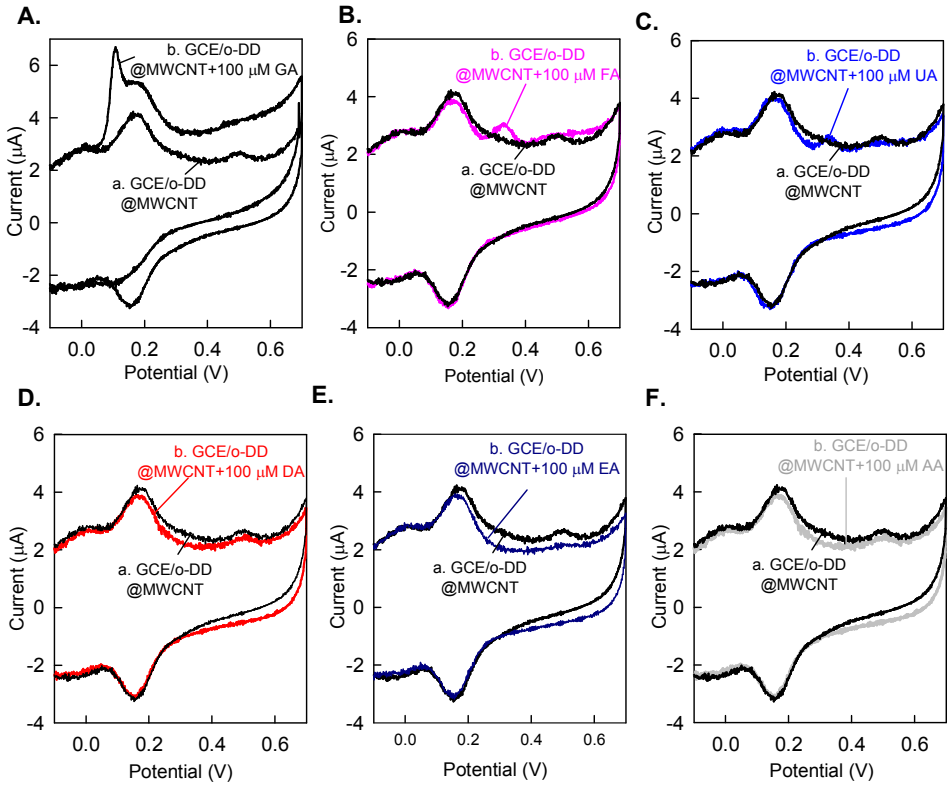

Figure 6

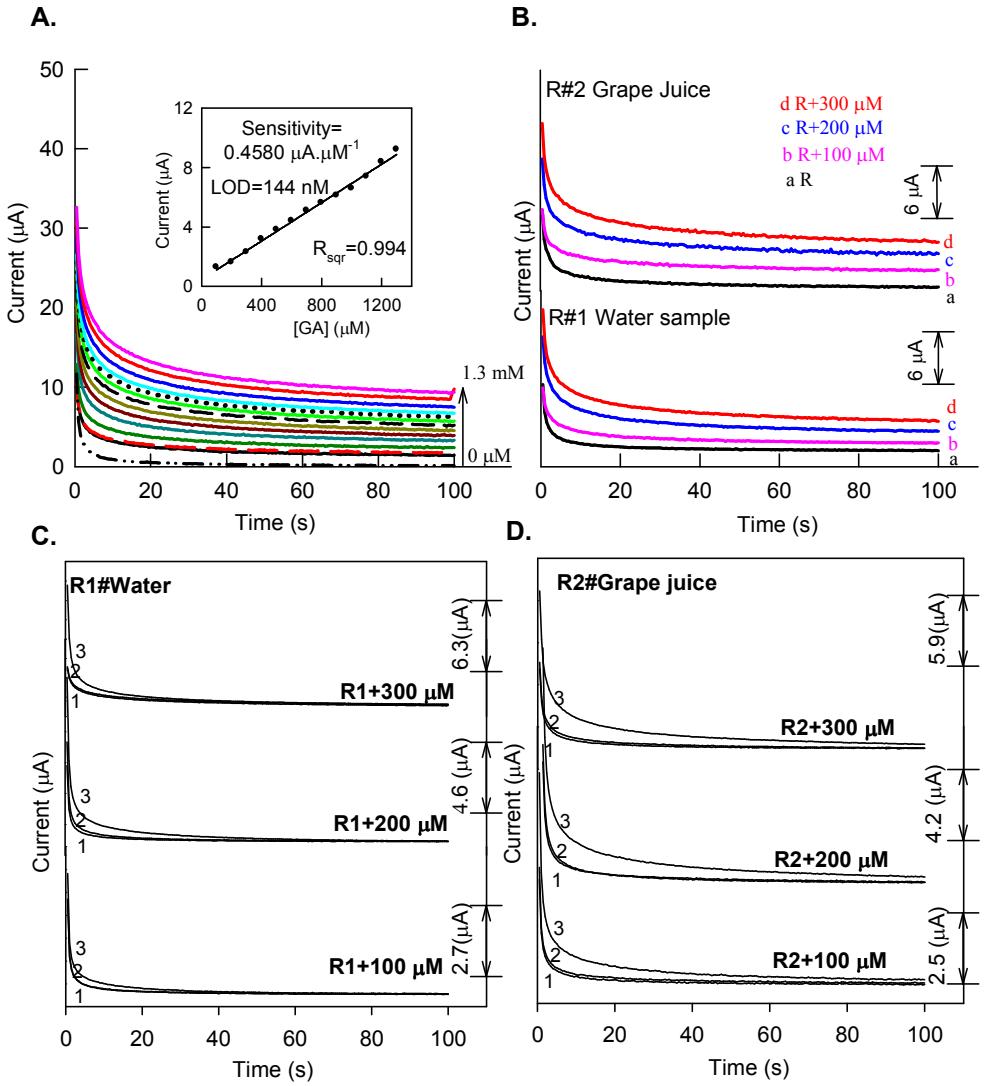

Table 1. Comparative results of the GA detection on various electrodes

S. No.	Electrode	pH	Detection Potential (V)	LOD (nM)	Linear range (µM)	Ref.
1	GCE/PEI-rGO[$]	1.55	0.50	300	0.58-580	[21]
2	CPE/MWCNT[@]	2.00	0.525	270	1-6.25	[27]
3	GCE	3.30	0.47	-	-	[28]
4	GE/TH/NiHCF*	7.00	0.40	1660	4.99-1200	[29]
5	MCPE[^]/CNT	2.50	0.35	300	0.5-150	[30]
6	GCE/PEP[&]	1.88	0.53	66.3	1-20	[31]
7	GCE-Tyr-nAu[#]	7.40	-0.10	700	25-900	[32]
8	SPE-Au-SAM/AuNPs-Linker/Fullerenol-TvL[%]	4.50	-0.10	600	30-300	[33]
9	`SiO_2nano/CPE	1.7	0.55	250	0.8-100	[34]
10	GCE/*o*-DD @MWCNT	7.00	0.16	144	100-1300	This work

[$]PEI-polyethyleneimine, rGO-functionalized graphene oxide;
[@] CPE-carbon paste electrode, CNT-multiwalled carbon nanotube;
*GE-graphite electrode, TH-thionine, NiHCF-nickel hexacyanoferrate;
[^] - modified carbon paste electrode;[&]PEP-polyephineprine;
[#]-Tyr-tyrosinase, nAu-gold nanoparticle.
[%]-SPE-Au- gold screen printed electrode, AuNPs-gold nanoparticles, TvL-trametes versicolor laccase;
`-Silicon dioxide nanoparticles.

Table 2. Results of GA detection in real samples

Real Sample[a]	Concentration (μM)			Apparent Recovery (%)
	Original	Spiked[b]	Detected[c]	
1. Grape Juice (#1)	0	100	99.65	99.65
		200	200.24	100.12
		300	298.94	99.65
2. Water (#2)	0	100	100.36	100.36
		200	200.09	100.05
		300	300.49	100.16

[a]. Dilution factor = 3 .
[b]. Real sample + Standard [GA].
[c]. Based on chronoamperometry at GCE/*o*-DD@MWCNT.